

Computational Fluid Dynamics Simulation of Daytime and Nighttime Summer Temperatures in 23 Special Wards of Tokyo

Project Representative

Yasunobu Ashie

National Institute for Land and Infrastructure Management

Authors

Yasunobu Ashie

National Institute for Land and Infrastructure Management

Takaaki Kono

Building Research Institute

Keiko Takahashi

The Earth Simulator Center, Japan Agency for Marine-Earth Science and Technology

Computational fluid dynamics simulations of air temperature fields were performed in the entire area of 23 special wards of Tokyo at 05:00, 14:00, and 22:00 local standard time on July 31, 2005. Comparisons with simulation results and observations showed the same tendency in the air temperature distributions at 14:00 and 22:00, where air temperatures in the coastal areas were cooler than those in the inland areas; while at 5:00, air temperatures in the coastal areas were hotter than those in the inland areas. The root mean square errors of air temperature between simulation results and observations were 0.5°C at 05:00, 1.1°C at 14:00, and 0.4°C at 22:00, respectively.

Keywords: urban heat island, CFD, air temperature, daytime and nighttime, summer, 23 special wards of Tokyo

1. Introduction

Recently, countermeasures against the urban heat island (UHI) effect, such as reduction of anthropogenic heat release and enhancement of urban ventilation, have become increasingly important in Tokyo. Evaluations of urban ventilation require construction of a high-resolution computational fluid dynamics (CFD) system, which takes into account complex urban morphology. The morphological complexity arises from multiscale geometry consisting of buildings, forests, and rivers, which is superimposed on varying topography. Given this morphological background, we have been developing a high-resolution CFD system and have performed simulations of wind and air temperature fields in the 23 special wards of Tokyo using a horizontal grid spacing of 5 m^[1]. In fiscal year 2009, we performed CFD simulations of daytime and nighttime summer temperature fields in the wards and compared the results with the actual observations.

2. Date and time of analysis

The CFD simulations were performed for 05:00, 14:00, 22:00 local standard time on July 31, 2005. This date was selected for two reasons. First, the UHI effect becomes the most severe during the day in summer. Second, the results of the current analysis can be compared against large-scale simultaneous meteorological observations—Metropolitan Environmental Temperature and Rainfall Observation System (METROS)

managed by Tokyo Metropolitan Government. In this study, air temperature data of METROS, observed at Stevenson screens located at elementary schools across Tokyo's 23 wards, are used. Figure 1 shows the horizontal computational domain of

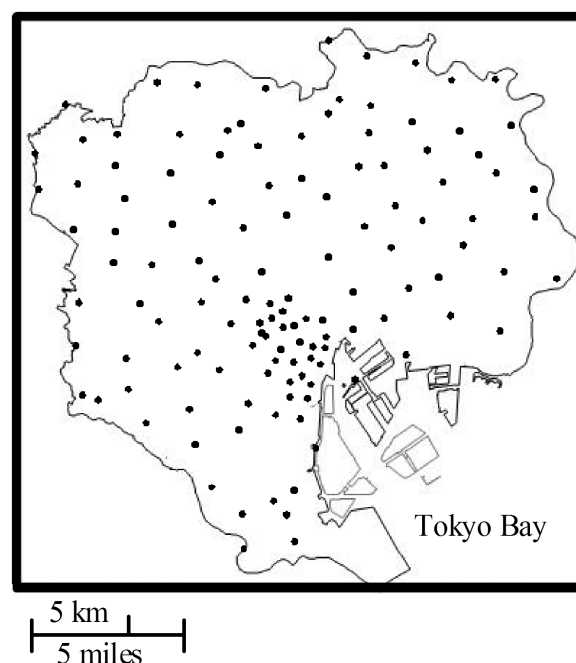


Fig. 1 Horizontal computational domain. Black dots indicate observation points (METROS).

33 km × 33 km. In the figure, observation points of METROS are indicated by black dots.

3. Calculation of surface temperatures

Although it is desirable to estimate the surface temperatures of buildings and other objects on the ground by performing a fully coupled conduction, radiation, and convection heat transfer simulation in three-dimensional space, the following simplified method is adopted in the present study. First, an unsteady heat conduction analysis is performed for individual cover types, which include asphalt and grassland. In the analysis, one-dimensional vertical heat conduction is assumed and evaluated according to the meteorological condition on the day of the simulation. The surface temperature of a cover type is calculated for both, the case with no shading from the sun and the case with shading from the sun. Subsequently, from the solar position at the hour of the analysis, the sunlit and shaded conditions of the urban surfaces are determined in every grid cell of the three-dimensional computational domain. The sunlit and shaded conditions of the urban surfaces are determined by taking into account the building arrangement within the city to be investigated by the CFD analysis. Finally, the surface temperature of the urban surface within an individual grid cell is assigned according to the surface cover types and the sunlit and shaded conditions.

When the surface-heat energy budget is solved, values for parameters such as albedo, emissivity, and evaporation efficiency are required. Ichinose et al. (1999)^[2] evaluated values for five parameters relevant to the surface-heat energy budget (i.e., albedo, evaporation efficiency, density, specific heat, and thermal diffusion coefficient) of 10 land cover types. Ihara et al. (2003)^[3] evaluated values for a different set of five parameters relevant to the surface-heat energy budget (i.e., albedo, emissivity, thermal diffusion coefficient, heat capacity, and thermal conductivity) of eight land cover types. This study uses relevant parameters and corresponding values from Ichinose et al. (1999)^[2] and Ihara et al. (2003)^[3]. These are summarized in

Table 1. Although the thermal diffusivity value is influenced by wind speed, it is set at a constant of $11.6 \text{ W m}^{-2} \text{ K}^{-1}$ (Yoshida et al., 2000)^[4]. The mass transfer coefficient is estimated using Lewis's law.

The surface temperatures of buildings and other objects on the grounds are estimated by performing a heat balance analyses using the parameters in Table 1 and meteorological observation data (AMeDAS, Tokyo); the estimated surface temperatures are used as boundary conditions for CFD simulations.

4. Comparisons of simulation results with observations

Figure 2 compares the horizontal distribution of the air temperature at 126 points of METROS from simulation results with those from METROS's observations. Here, simulation results at 2 m above the ground are depicted. In addition, data at a point over the sea ($35^{\circ} 27' 52.09'' \text{ N}$, $139^{\circ} 52' 28.35'' \text{ E}$) observed by Ministry of Environment (MOE)^[5] are depicted. At 05:00 in Fig. 2 (a), air temperatures in the coastal areas are higher than those in the inland areas. At 14:00 in Fig. 2 (b), air temperatures are lower in the eastern areas and higher in the central and northern areas of the inland. At 22:00 in Fig. 2 (c), air temperatures of the north side of inland areas and those of the central areas obviously become higher than those of other areas and form an inverted triangular shaped region of higher temperature. Simulation results and observations are almost identical. The root mean square errors of air temperature between simulation results and observations are 0.5°C at 05:00, 1.1°C at 14:00, and 0.4°C at 22:00, respectively.

Figure 3 shows the frequency distributions of the maximum differences in the simulated air temperatures within an area of $100 \text{ m} \times 100 \text{ m}$ at and around each observation point. At 05:00 and 22:00, areas with the maximum air temperature differences within 1°C account for 90 percent or more. However, at 14:00, areas with the maximum air temperature differences above 1°C account for 90 percent or more, indicating a great unevenness in air temperature distributions.

Table 1 Values of parameters relevant to the surface energy budget

Land use classification adopted for the present study	Building sites	Asphalt	Grassland	Water	Trees
Albedo [-] (Ichinose et al. 1999)	0.18	0.18	0.16	0.08	0.16
Surface emissivity [-] (Ihara et al. 2003)	0.96	0.91	0.95	0.93	0.95
Evaporation efficiency [-] (Ichinose et al. 1999)	0.05	0.05	0.30	1.00	0.30
Density [kg m^{-3}] (Ichinose et al. 1999)	2.4×10^3	2.1×10^3	1.8×10^3	1.0×10^3	1.8×10^3
Specific heat [$\text{J kg}^{-1} \text{K}^{-1}$] (Ichinose et al. 1999)	882	882	1176	4200	1176

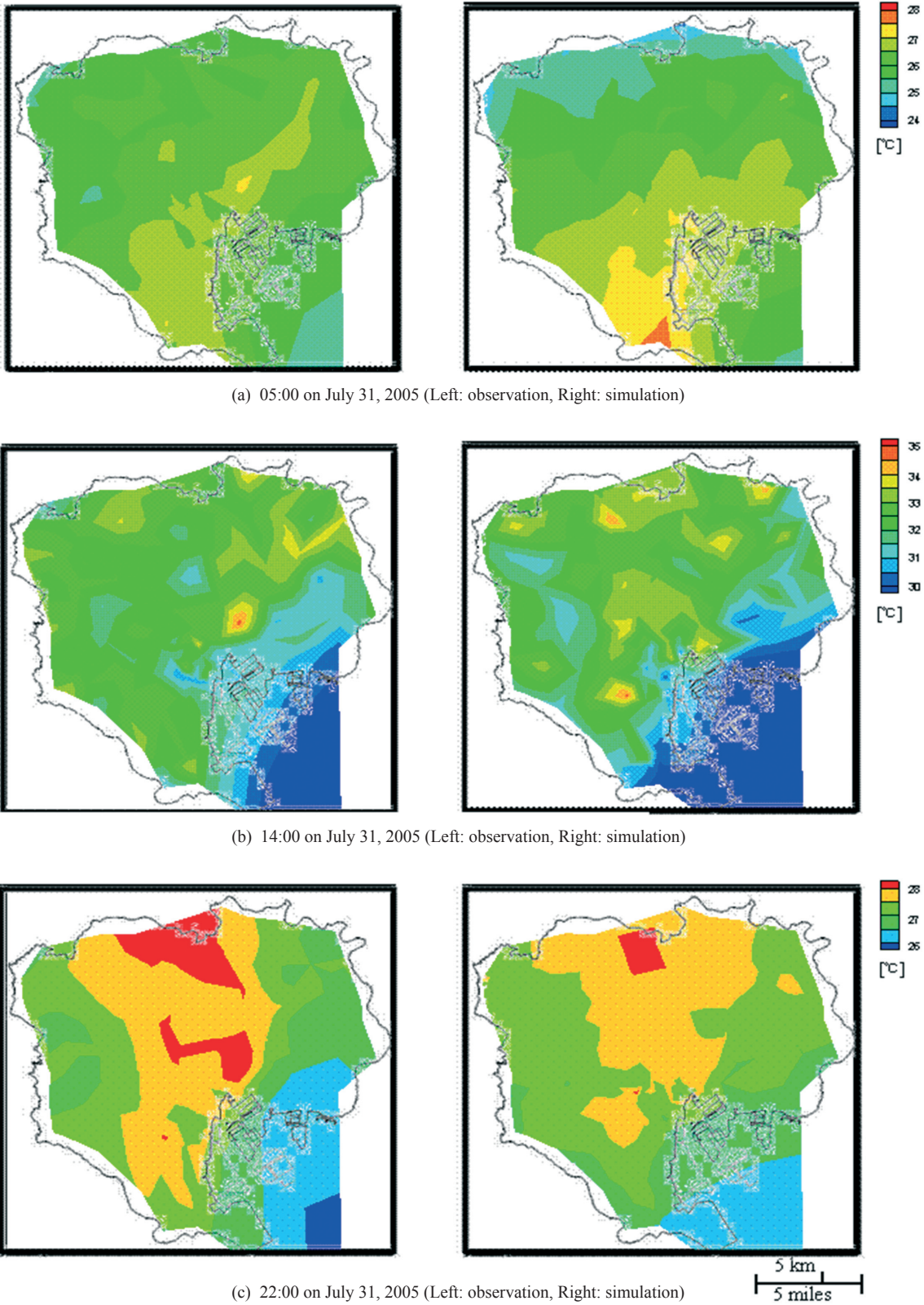


Fig. 2 Horizontal distribution of air temperature
Observation: observation data at 126 METROS observation points and one MOE observation point^[5]. Simulation: simulation results at 2 m above the ground at the observation points.

5. Future work

Figure 4 shows the pathlines of fluid particles that flow through the points at $Y = 18000$ m with 3000 m spacing in the X direction and 50 m spacing in the Z direction from $Z = 50$ m to 250 m at 05:00. Here, the color of the pathline indicates air temperature. Wind direction prevails from the north at $Y = 33000$ m. The figure shows that the pathlines reach near the height of the computational domain ($Z = 500$ m) in the region of 27°C or higher in Fig. 2 (a, Right). It is possible that the

overestimation of air temperature in this region is caused by the suppression of vertical mixing of heat due to the influence of the upper computational domain. The same symptom is confirmed in the distribution of pathlines at 14:00 (not shown here).

Therefore, we believe that to improve the reproducibility of the air temperature distribution, it is important to improve the reproducibility of the development of the atmospheric boundary layer. In the future, we plan to improve our simulation model to be able to deal with unsteady-state conditions. In addition, we

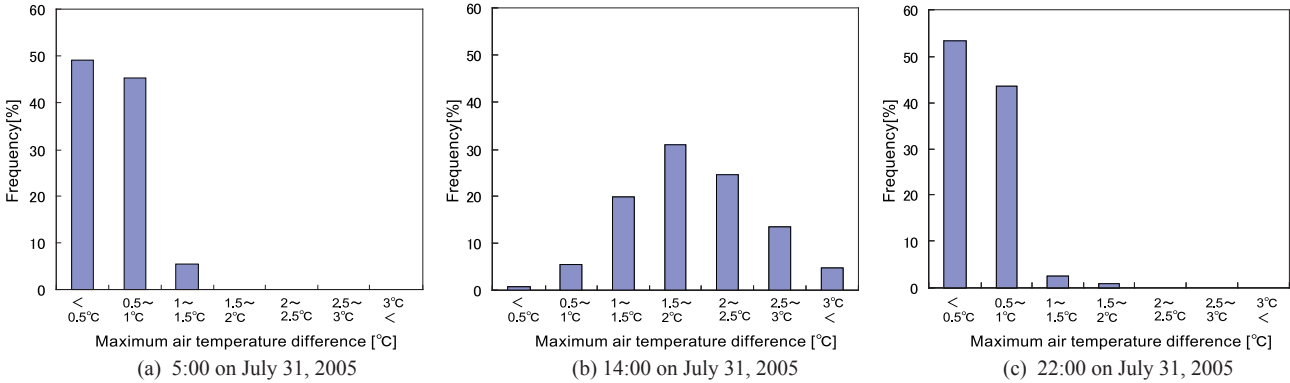


Fig. 3 Frequency distribution of the maximum difference in the simulated air temperatures in areas of $100\text{ m} \times 100\text{ m}$ at and around the observation points. (2 m above the ground).

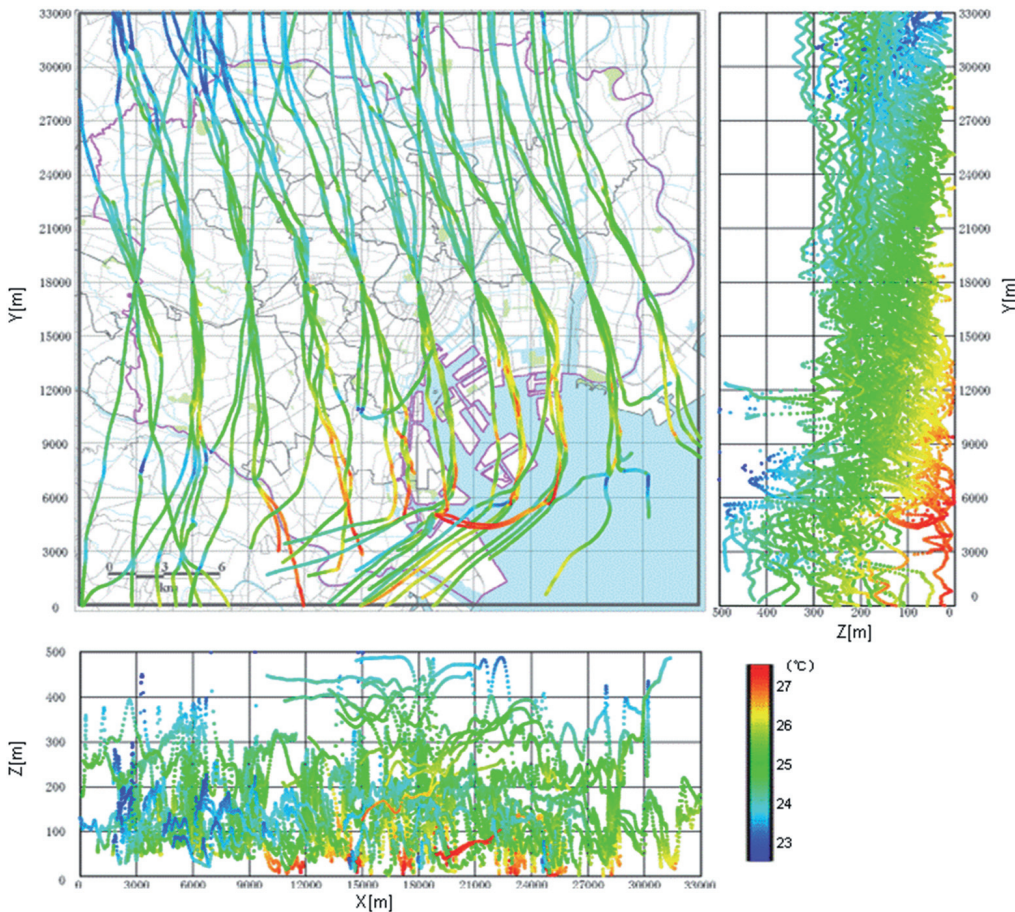


Fig. 4 Pathline distribution at 05:00 on July 31, 2005 (trajectory of a fluid particle that flows through points at $Y = 18000$ m with 3000 m spacing in the X direction and 50 m spacing in the Z direction from $Z = 50$ m to 250 m).

are planning to study the influence of the upper boundary of a computational domain.

6. Summary

We performed CFD simulations of air temperature fields in the entire area of the 23 special wards of Tokyo at 05:00, 14:00, and 22:00. By comparing the simulation results and the observations, we confirmed that both show the same air temperature distribution tendencies: at 14:00 and 22:00, air temperatures in the coastal areas were cooler than those in the inland areas; while at 05:00, air temperatures in the coastal areas were hotter than those in the inland areas. The root mean square errors of air temperature between simulation results and observations were 0.5°C at 05:00, 1.1°C at 14:00, and 0.4°C at 22:00, respectively.

References

- [1] K. Hirano, T. Kono, and Y. Ashie: "Large-scale CFD simulation of heat island phenomenon and countermeasures in Tokyo," Annual report of the earth simulator center April 2007-March 2008, The Earth Simulator Center (JAMSTEC), 2008.
- [2] T. Ichinose, K. Shimodozono, and K. Hanaki: "Impact of anthropogenic heat on urban climate in Tokyo," *Atmospheric Environment* 33: 3897-3909, 1999.
- [3] T. Ihara, H. Aida, Y. Yoshida, T. Handa, R. Matsushashi, and H. Ishitani: "Evaluation of CO₂ Emissions Reduction Effect from the Building by Introducing High Light-Reflective and High Heat-Emissive Paint considering Urban Thermal Environment," Proc. 19th conf. on energy, Economy, and Environment, 655-660, 2003. (in Japanese)
- [4] S. Yoshida, S. Murakami, A. Mochida, R. Ooka, Y. Tominaga, and S. Kim: "Influence of green area ratio on outdoor thermal environment with coupled simulation of convection, radiation and moisture transport," *Journal of architecture planning and environmental engineering, Transactions of AIJ* 529: 77-84, 2000. (in Japanese)
- [5] Ministry of Environment: http://www.env.go.jp/air/life/heat_island/wm/index.html

東京 23 区の夏期昼夜間における熱環境の数値シミュレーション

プロジェクト責任者

足永 靖信 国土技術政策総合研究所

著者

足永 靖信 国土技術政策総合研究所

河野 孝昭 建築研究所

高橋 桂子 海洋研究開発機構 地球シミュレータセンター

東京 23 区全域を対象にして臨海部から内陸に至る 33km 四方の領域の熱環境について CFD 解析を実施した。個々の建築物を陽的に解像する為に水平メッシュ解像度を 5m とし、総メッシュ数は約 50 億である。夏期の 3 時刻 (5 時、14 時、22 時) を対象にして解析を行い得られた気温分布を 127 点の観測値と比較した。各時刻の気温分布は観測と計算がほぼ一致した傾向を示し、内陸と比較すると 14 時と 22 時には湾岸地域の気温が低く、5 時には湾岸地域の気温が逆に高かった。RMS 誤差は 5 時 : 0.5℃、14 時 : 1.1℃、22 時 : 0.4℃であった。風速の計算結果を用いて流跡線を作成し、東京 23 区における昼夜間の 3 次元的な流れ構造を検討した。ただし、今回の CFD 解析は定常状態を仮定しているため、より現実に近い条件で検討を進めるためには、モデルの非定常化を行うとともに、適切な解析領域高さを設定する必要がある。

キーワード: ヒートアイランド, CFD, 気温, 昼夜, 夏期, 東京 23 区